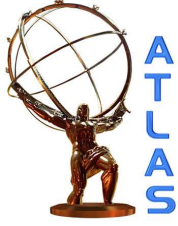
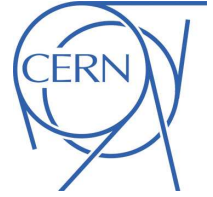


EUROPEAN ORGANISATION FOR NUCLEAR RESEARCH (CERN)



Submitted to: Phys. Lett. B.

CERN-PH-EP-2016-026
1st March 2016

Search for new phenomena in final states with large jet multiplicities and missing transverse momentum with ATLAS using $\sqrt{s} = 13$ TeV proton–proton collisions

The ATLAS Collaboration

Abstract

Results are reported of a search for new phenomena, such as supersymmetric particle production, that could be observed in high-energy proton–proton collisions. Events with large numbers of jets, together with missing transverse momentum from unobserved particles, are selected. The data analysed were recorded by the ATLAS experiment during 2015 using the 13 TeV centre-of-mass proton–proton collisions at the Large Hadron Collider, and correspond to an integrated luminosity of 3.2 fb^{-1} . The search selected events with various jet multiplicities from ≥ 7 to ≥ 10 jets, and with various b -jet multiplicity requirements to enhance sensitivity. No excess above Standard Model expectations is observed. The results are interpreted within two supersymmetry models, where gluino masses up to 1400 GeV are excluded at 95% confidence level, significantly extending previous limits.

1 Introduction

New strongly interacting particles, if present at the TeV energy scale, may be produced in high-energy proton–proton (pp) collisions and decay to final states with large jet multiplicities. If their decay produces stable particles which only interact weakly, it will also result in a momentum imbalance in the plane transverse to the beam (\vec{E}_T^{miss}).

Such particles are present in supersymmetry (SUSY) [1–6], a theoretically favoured extension of the Standard Model (SM) that predicts partner fields for each of the SM particles. These fields combine into physical superpartners of the SM particles. The scalar partners of quarks and leptons are known as squarks (\tilde{q}) and sleptons ($\tilde{\ell}$). The fermionic partners of gauge and Higgs bosons are the gluinos (\tilde{g}), the charginos ($\tilde{\chi}_i^\pm$, with $i = 1, 2$) and the neutralinos ($\tilde{\chi}_i^0$ with $i = 1, 2, 3, 4$), with $\tilde{\chi}_i^\pm$ and $\tilde{\chi}_i^0$ being the mass eigenstates, ordered from the lightest to the heaviest, formed from the linear superpositions of the SUSY partners of the Higgs and electroweak gauge bosons.

Under the hypothesis of R -parity conservation [7], SUSY partners are produced in pairs and decay to the lightest supersymmetric particle (LSP), which is stable and in a large variety of models is assumed to be the lightest neutralino ($\tilde{\chi}_1^0$), which escapes detection. The undetected $\tilde{\chi}_1^0$ would result in missing transverse momentum, while the rest of the cascade can yield final states with multiple jets and possibly leptons and/or photons. The strongly interacting gluinos and squarks can have large production cross-sections at the Large Hadron Collider (LHC), but no evidence of their existence has been observed to date.

This paper presents the results of a search for new phenomena, such as supersymmetry, in final states with large jet multiplicities (from ≥ 7 to ≥ 10 jets) in association with E_T^{miss} . This signature is exhibited, for example, by squark and gluino production followed by cascade decay chains, and/or decays to heavy SM particles, such as top quarks or W , Z or Higgs bosons, each of which can produce multiple jets in their decays. In contrast to many other searches for the production of strongly interacting SUSY particles, the requirement made here of large jet multiplicity means that the requirement on E_T^{miss} can be modest.

Previous searches [8–10] in similar final states have been performed by the ATLAS Collaboration at the lower centre-of-mass energies of $\sqrt{s} = 7$ TeV and 8 TeV, with integrated luminosities up to 20.3 fb^{-1} . The larger energy of the present dataset provides increased sensitivity, particularly to particles with higher masses. This paper closely follows the strategy of those previous studies. In particular, data are collected using an online selection relying only on high jet multiplicity and the signal regions (SR) are designed such that the dominant multijet background can be determined from the data using regions of lower E_T^{miss} and/or lower jet multiplicity.

The data were collected by the ATLAS detector [11] in pp collisions at the LHC at a centre-of-mass energy of 13 TeV, from 16th August to 3rd November 2015. The detector covers the pseudorapidity¹ range of $|\eta| < 4.9$ and is hermetic in azimuth. It consists of an inner tracking detector surrounded by a superconducting solenoid, electromagnetic and hadronic calorimeters, and an external muon spectrometer incorporating large superconducting toroidal magnets. After applying beam-, data- and detector-quality criteria, the integrated luminosity was $3.2 \pm 0.2 \text{ fb}^{-1}$. The uncertainty was derived using beam-separation scans, following a methodology similar to that detailed in Ref. [12].

¹ ATLAS uses a right-handed coordinate system with its origin at the nominal interaction point (IP) in the centre of the detector and the z -axis along the beam pipe. Cylindrical coordinates (r, ϕ) are used in the transverse plane, ϕ being the azimuthal angle around the beam pipe. The transverse momentum of a four-momentum is $\vec{p}_T = (p_x, p_y)$, its rapidity is $y = \frac{1}{2} \ln \frac{E+p_z}{E-p_z}$, and the pseudorapidity is defined in terms of the polar angle θ as $\eta = -\ln \tan(\theta/2)$.

2 Physics object definition

Jets are reconstructed using the anti- k_t clustering algorithm [13, 14] with jet radius parameter $R = 0.4$ and starting from clusters of calorimeter cells [15]. The effects of coincident pp interactions (‘pileup’) on jet energies are accounted for by an event-by-event p_T -density correction [16]. The energy resolution of the jets is improved by using global sequential calibrations [17, 18]. Events with jets originating from cosmic rays, beam background and detector noise are vetoed using the ‘loose’ requirements of Ref. [19]. Jets containing b -hadrons (b -jets) are identified using an algorithm exploiting the long lifetime, high decay multiplicity, hard fragmentation and large mass of b -hadrons [20]. The b -tagging algorithm tags b -jets with an efficiency of approximately 70% in simulated $t\bar{t}$ events, and mis-tags c -jets, τ -jets and light-quark or gluon jets with probabilities of approximately 10%, 4% and 0.2% respectively [21].

The primary vertex (PV) in each event is the vertex with the largest value of Σp_T^2 for all tracks associated with it. To reduce the effect of pileup, a jet having $20 \text{ GeV} < p_T < 50 \text{ GeV}$ and $|\eta| < 2.4$ is disregarded when the p_T -weighted sum of its associated tracks indicates that it originated from a pileup collision and not the PV, based on a jet vertex tagger as described in Ref. [16].

Electron candidates are identified according to the likelihood-based ‘loose’ criterion described in Ref. [22], formed from e.g. calorimeter shower shape and inner-detector track properties. Muon candidates are identified according to the ‘medium’ criterion described in Ref. [23], based on combined tracks from the inner detector and muon spectrometer. These candidates (which may cause an event to be rejected from the signal regions) are required to have $p_T > 10 \text{ GeV}$, $|\eta| < 2.47$ for e and $|\eta| < 2.5$ for μ .

To avoid double-counting of reconstructed objects, electron candidates sharing an inner-detector track with a muon candidate are removed. Next, jet candidates separated from an electron candidate by $\Delta R_y < 0.2$ are removed, where $\Delta R_y = \sqrt{(\Delta y)^2 + (\Delta \phi)^2}$. Jet candidates with fewer than three tracks and with $\Delta R_y < 0.4$ from a muon candidate are then removed. Following this, any lepton candidate separated from a surviving jet candidate by $\Delta R_y < 0.4$ is removed.

The missing transverse momentum, \vec{E}_T^{miss} , is the negative two-vector sum of the calibrated \vec{p}_T of reconstructed jets with $p_T > 20 \text{ GeV}$ and $|\eta| < 4.5$, electrons, muons and photons [24]. It includes an additional contribution from inner-detector tracks, matched to the PV, that are not associated with these reconstructed objects. Photons are not considered beyond their contribution to the \vec{E}_T^{miss} unless they are reconstructed as jets. To reduce the effect of pileup, jets do not contribute to the \vec{E}_T^{miss} calculation when they are disregarded based on the jet vertex tagger as described above. Additionally, when a jet having $50 \text{ GeV} < p_T < 70 \text{ GeV}$, $|\eta| < 2.0$ and azimuth relative to the missing momentum $\Delta\phi(\vec{p}_T, \vec{E}_T^{\text{miss}}) > 2.2$ meets the same vertex-tagging criterion, the event is discarded. Events in which the jet closest in ϕ to the \vec{E}_T^{miss} is found in or near an inactive region in the hadronic calorimeter barrel (i.e. $-0.1 < \eta < 1.0$, $0.8 < \phi < 1.1$) are also discarded, in order to reduce the impact of this source of \vec{E}_T^{miss} mismeasurement. These data-quality requirements reduce the expected acceptance of typical SUSY models by approximately 5%.

When defining leptons for control regions (Section 5), the candidates defined above are required to be isolated, to have a longitudinal impact parameter z_0 (with respect to the PV) satisfying $|z_0 \sin \theta| < 0.5 \text{ mm}$, and to have the significance of their transverse impact parameter $|d_0/\sigma(d_0)|$ (with respect to the measured beam position) be less than five for electrons and less than three for muons. Additionally, electrons must satisfy the ‘tight’ criterion of Ref. [22].

3 Event selection

The signal regions are defined using two jet multiplicity counts: either n_{50} , the number of jets having $p_T > 50$ GeV and $|\eta| < 2.0$, or n_{80} , the number of such jets which additionally satisfy the higher requirement $p_T > 80$ GeV. The online selection (trigger) for n_{50} -based regions requires events to have at least six jets each with $p_T > 45$ GeV and $|\eta| < 2.4$, while that for n_{80} -based regions requires at least five jets each with $p_T > 70$ GeV. The trigger efficiency is greater than 99.5% for events satisfying the signal selection described below. Jets with a looser definition – those having $p_T > 40$ GeV and $|\eta| < 2.8$ – are used to construct the scalar sum $H_T = \sum p_T^{\text{jet}}$, while those having $p_T > 40$ GeV and $|\eta| < 2.5$ are candidates for b -tagging, contributing to the number $n_{b\text{-jet}}$ of b -tagged jets.

The signal selection requires large jet multiplicity, which depends on the signal region (SR), as shown in Table 1. Fifteen different SRs are defined, providing wide-ranging sensitivity to models with different final states and mass spectra. There are three different triplets of regions defined in terms of the jet multiplicity n_{50} and two different triplets of regions defined in terms of n_{80} . Within each triplet, different requirements are made on $n_{b\text{-jet}}$, from no requirement to the requirement of at least two b -jets. In all cases the final selection is on the ratio of E_T^{miss} to $\sqrt{H_T}$, with the choice of a threshold at $4 \text{ GeV}^{1/2}$ being a good balance between background rejection and signal efficiency while maintaining the effectiveness of the background estimation. Events containing electron or muon candidates with $p_T > 10$ GeV are vetoed to reduce background from SM processes.

The SRs have events in common, for example all events in 9j50-1b also appear in 9j50, which does not require the b -jet, and in 8j50 and 8j50-1b, which have a looser requirement on n_{50} . Events may also appear in both the n_{50} and the n_{80} categories.

4 Background and simulation

Standard Model processes contribute to the event counts in the SRs. The dominant background contributions are multijet production, including those from purely strong interaction processes and fully hadronic

	8j50	8j50-1b	8j50-2b	9j50	9j50-1b	9j50-2b	10j50	10j50-1b	10j50-2b
n_{50}	≥ 8			≥ 9			≥ 10		
$n_{b\text{-jet}}$	—	≥ 1	≥ 2	—	≥ 1	≥ 2	—	≥ 1	≥ 2
$E_T^{\text{miss}} / \sqrt{H_T}$	$> 4 \text{ GeV}^{1/2}$								

(a) Signal regions using n_{50} .

	7j80	7j80-1b	7j80-2b	8j80	8j80-1b	8j80-2b
n_{80}	≥ 7			≥ 8		
$n_{b\text{-jet}}$	—	≥ 1	≥ 2	—	≥ 1	≥ 2
$E_T^{\text{miss}} / \sqrt{H_T}$	$> 4 \text{ GeV}^{1/2}$					

(b) Signal regions using n_{80} .

Table 1: Definition of the signal regions. The selection variables are described in Sections 2 and 3. A long dash ‘—’ indicates that no requirement is made. Events with leptons are vetoed.

decays of $t\bar{t}$; partially leptonic decays of $t\bar{t}$; and leptonically decaying W or Z bosons produced in association with jets. Top-quark, W - and Z -boson decays that are not fully hadronic are collectively referred to as ‘leptonic’ backgrounds. They can contribute to the signal regions when no e or μ leptons are produced, for example $Z \rightarrow \nu\nu$ or hadronic $W \rightarrow \tau\nu$ decays, or when they are produced but are out of acceptance, lie within jets, or are not reconstructed.

The most significant leptonic backgrounds are $t\bar{t}$ and W boson production in association with jets. The contribution of these two backgrounds to the signal regions is determined from a combined fit as described later in Section 5. The yields for the other, generally subdominant, leptonic backgrounds are taken from the simulations as described below.

Monte Carlo simulations are used in the determination of the leptonic backgrounds and to assess sensitivity to specific SUSY signal models. All simulated events are overlaid with multiple pp collisions simulated with the soft QCD processes of PYTHIA 8.186 [25] using the A2 set of parameters (tune) [26] and the MSTW2008LO parton distribution functions (PDF) [27]. The simulations are weighted such that the pileup conditions match those of the data. The response of the detector to particles is modelled with an ATLAS detector simulation [28] based fully on GEANT4 [29], or using fast simulation based on a parameterisation of the performance of the ATLAS electromagnetic and hadronic calorimeters [30] and on GEANT4 elsewhere. Leptonic background samples use full simulation, while signal samples (described below) use the fast simulation option. Corrections are applied to the simulated samples to account for differences between data and simulation for the lepton identification and reconstruction efficiencies, and for the efficiency and misidentification rate of the b -tagging algorithm.

4.1 Leptonic background simulation

For the generation of $t\bar{t}$ and single top quarks in the Wt and s -channels [31] Powheg-Box v2 [32] is used with the CT10 PDF sets [33] in the matrix element calculations. Electroweak t -channel single-top-quark events are generated using Powheg-Box v1. This generator uses the four-flavour scheme for the next-to-leading order (NLO) matrix element calculations together with the fixed four-flavour PDF set CT10f4 [33]. For this process, the top quarks are decayed using MadSpin [34] preserving all spin correlations, while for all processes the parton shower, fragmentation, and the underlying event are simulated using PYTHIA v6.428 [35] with the CTEQ6L1 PDF sets [36] and the corresponding Perugia 2012 tune (P2012) [37]. The top quark mass is set to 172.5 GeV. The EvtGen v1.2.0 program [38] models the bottom and charm hadron decays, as it does for all non-SHERPA-simulated processes mentioned below. The $t\bar{t}$ simulation is normalised to the cross-section calculated to next-to-next-to-leading order (NNLO) in perturbative QCD, including soft-gluon resummation to next-to-next-to-leading-log (NNLL) accuracy [39].

Events containing $t\bar{t}$ and additional heavy particles – comprising three-top, four-top, $t\bar{t} + W$, $t\bar{t} + Z$ and $t\bar{t} + WW$ production [40] – are simulated at leading order in the strong coupling constant α_s , using MadGraph v2.2.2 [41] with up to two additional partons in the matrix element, interfaced to the PYTHIA 8.186 [25, 35] parton shower model. The A14 tune of the PYTHIA parameters is used [42], together with the NNPDF2.3LO PDF set [43]. The predicted production cross-sections are calculated to NLO as described in Ref. [41] for all processes other than three-top, for which it is calculated to LO.

Events containing W bosons or Z bosons with associated jets [44] are likewise simulated using MadGraph, but with up to four additional final-state partons in the matrix element, and interfaced to PYTHIA, using the same tunes and particle decay programs. The $W + \text{jets}$ and $Z + \text{jets}$ events are normalised to NNLO

cross-sections [45]. Diboson processes with at least one boson decaying leptonically [46] are simulated using the SHERPA v2.1.1 generator [47]. The matrix element calculations contain all diagrams with four electroweak vertices. They are calculated for up to one (for 4ℓ , $2\ell+2\nu$, semileptonic ZZ) or no additional partons (for $3\ell+1\nu$, other semileptonic processes) at NLO and up to three additional partons at LO using the Comix [48] and OpenLoops [49] matrix element generators and interfaced with the SHERPA parton shower [50] using the ME+PS@NLO prescription [51]. The CT10 PDF set is used in conjunction with dedicated parton shower tuning developed by the SHERPA authors.

Theoretical uncertainties are considered for all these simulated samples. Production of $t\bar{t}$ is by far the most important process simulated in this analysis and to evaluate the uncertainty on this background several samples are compared. Samples are produced with the factorisation and renormalisation scales varied coherently, along with variations of the resummation damping parameter and with more/less radiation tunes of the parton shower [52]. Additionally the nominal sample is compared to one with Powheg interfaced with Herwig++ [53] and SHERPA v2.1.1 samples with up to one additional jet at next-to-leading order using OpenLoops and up to four additional jets at leading order, to account for uncertainties in the parton shower and the generator respectively. The comparison with the SHERPA sample dominates the uncertainty in the signal region prediction.

4.2 SUSY signal models

Two classes of SUSY signal models are used when interpreting the results. The first is a simplified model, in which gluinos are pair-produced and then decay via the cascade

$$\begin{aligned}\tilde{g} &\rightarrow q + \bar{q}' + \tilde{\chi}_1^\pm \quad (q = u, d, s, c) \\ \tilde{\chi}_1^\pm &\rightarrow W^\pm + \tilde{\chi}_2^0 \\ \tilde{\chi}_2^0 &\rightarrow Z + \tilde{\chi}_1^0.\end{aligned}$$

The parameters of the model are the masses of the gluino, $m_{\tilde{g}}$, and the lightest neutralino, $m_{\tilde{\chi}_1^0}$. The mass of the $\tilde{\chi}_1^\pm$ is constrained to be $\frac{1}{2}(m_{\tilde{g}} + m_{\tilde{\chi}_1^0})$ and the mass of the $\tilde{\chi}_2^0$ to be $\frac{1}{2}(m_{\tilde{\chi}_1^\pm} + m_{\tilde{\chi}_1^0})$. All other sparticles are kinematically inaccessible. This model is labelled in the following figures as ‘2-step’.

A second set of SUSY models is drawn from a two-dimensional subspace (a ‘slice’) of the 19-parameter phenomenological Minimal Supersymmetric Standard Model (pMSSM) [54, 55]. The selection is motivated in part by models not previously excluded in the analysis presented in Ref. [56]. The models are selected to have a bino-dominated $\tilde{\chi}_1^0$, kinematically accessible gluinos, and a Higgsino-dominated multiplet at intermediate mass. The Higgsino multiplet contains two neutralinos (the $\tilde{\chi}_2^0$ and $\tilde{\chi}_3^0$) and a chargino (the $\tilde{\chi}_1^\pm$). The mass of these particles is varied by changing the soft SUSY-breaking parameters M_3 (for the gluino), M_1 (for the $\tilde{\chi}_1^0$, set to 60 GeV), and μ (for the Higgsinos). In order that other SUSY particles remain kinematically inaccessible, the other parameters, defined in Ref. [56], are set to $M_A = M_2 = 3$ TeV, $A_\tau = 0$, $\tan\beta = 10$, $A_t = A_b = m_{L(1,2,3)} = m_{(\tilde{e}, \tilde{\mu}, \tilde{\tau})} = m_{\tilde{Q}(1,2,3)} = m_{(\tilde{u}, \tilde{c}, \tilde{t})} = m_{(\tilde{d}, \tilde{s}, \tilde{b})} = 5$ TeV. Mass spectra with consistent electroweak symmetry breaking are generated using softsusy 3.4.0 [57]. The decay branching ratios are calculated with SDECAY/HDECAY 1.3b/3.4 [58], and when $m_{\tilde{\chi}_1^\pm} \lesssim 500$ GeV and $m_{\tilde{g}} \gtrsim 1200$ GeV the predominant decays are $\tilde{g} \rightarrow t + \bar{t} + \tilde{\chi}_{2,3}^0$ and $\tilde{g} \rightarrow t + \bar{b} + \tilde{\chi}_1^\pm$, with $\tilde{\chi}_{2,3}^0$ decaying to $Z/h + \tilde{\chi}_1^0$ and $\tilde{\chi}_1^\pm$ to $W^\pm + \tilde{\chi}_1^0$ (numerical values are provided in Ref. [59]). When these decays dominate they lead to final states with many jets, several of which are b -jets, but relatively little E_T^{miss} . This renders this search particularly sensitive compared to most other SUSY searches, which tend to require

high E_T^{miss} . At higher $m_{\tilde{\chi}_1^\pm}$ and lower $m_{\tilde{g}}$, the decay $\tilde{g} \rightarrow q + \bar{q} + \tilde{\chi}_1^0$ becomes dominant and this search starts to lose sensitivity. This model is labelled in the following figures as ‘pMSSM’.

The signal events are simulated using MadGraph v2.2.2 at LO interfaced to PYTHIA 8.186, as for those of W +jets and Z +jets. The signal cross-sections are calculated at NLO in the strong coupling constant, adding the resummation of soft gluon emission at next-to-leading-logarithmic (NLL) accuracy [60–64]. The nominal cross-section is taken from an envelope of cross-section predictions using different PDF sets and factorisation and renormalisation scales, as described in Ref. [65].

For the model points shown later in Figures 1–3, with $m_{\tilde{g}} = 1300$ GeV slightly beyond the Run-1 exclusion limits, the SR selection efficiencies are around 8% in the SRs most sensitive to those models.

4.3 Multijet background

The signal regions were chosen such that the background from the multijet process can be determined from the data. The method relies on the observation [8] that where E_T^{miss} originates predominantly from calorimeter energy mismeasurement, as is the case for the multijet contributions, the distribution of the ratio $E_T^{\text{miss}}/\sqrt{H_T}$ is almost invariant under changes in jet multiplicity. This invariance, which is illustrated in Figure 1, occurs because the calorimeter resolution that produces the momentum imbalance in these events is dominated by stochastic processes which have variance proportional to H_T , and is largely independent of the jet multiplicity.

The shape of the $E_T^{\text{miss}}/\sqrt{H_T}$ distribution is measured in control regions (CR) with lower jet multiplicities than the signal regions, and correspondingly much higher multijet contributions. For the n_{50} signal regions, the CR contains events with exactly six jets having $p_T > 50$ GeV. For the n_{80} signal regions, the CR requires exactly five jets with $p_T > 80$ GeV. For each SR jet selection, an appropriate $E_T^{\text{miss}}/\sqrt{H_T}$ distribution template is normalised to the data in a further CR having the same jet multiplicity as the SR but with $E_T^{\text{miss}}/\sqrt{H_T} < 1.5 \text{ GeV}^{1/2}$. That normalised template then provides the background prediction for the SR multiplicity in the region with $E_T^{\text{miss}}/\sqrt{H_T} > 4 \text{ GeV}^{1/2}$.

Since semileptonic b -hadron decays can contribute to E_T^{miss} , these $E_T^{\text{miss}}/\sqrt{H_T}$ template distributions are built separately for each $n_{b\text{-jet}}$ requirement. For example, the multijet contribution to the 9j50–1b signal region is determined using a template built from events with exactly six jets with $p_T > 50$ GeV, and $n_{b\text{-jet}} \geq 1$. That template is normalised to 9j50–1b in the region with $E_T^{\text{miss}}/\sqrt{H_T} < 1.5 \text{ GeV}^{1/2}$.

When constructing and normalising the $E_T^{\text{miss}}/\sqrt{H_T}$ templates, the same lepton veto is used as for the signal regions. However, some leptonic background contributions persist, and so the expected leptonic backgrounds to those templates (normalised according to their theoretical cross-sections, as described in Section 4.1) are subtracted from the data distributions. The uncertainties associated with the leptonic backgrounds are included in the systematic uncertainty in the prediction. Non-stochastic contributions to calorimeter resolution, which lead to a residual dependence of the $E_T^{\text{miss}}/\sqrt{H_T}$ distribution on H_T (at the $O(10\%)$ level), are reduced by constructing the templates in four bins of H_T in the kinematic region of interest. Those proto-templates are combined with weights which reflect the H_T distribution of the CR with the same jet multiplicity as the target SR but with $E_T^{\text{miss}}/\sqrt{H_T} < 1.5 \text{ GeV}^{1/2}$. The effect of changing the H_T binning is included in the systematic uncertainty.

The validity of assuming $E_T^{\text{miss}}/\sqrt{H_T}$ invariance is tested with data, using a series of validation regions (VR) with smaller jet multiplicities or smaller $E_T^{\text{miss}}/\sqrt{H_T}$ (between $1.5 \text{ GeV}^{1/2}$ and $3.5 \text{ GeV}^{1/2}$) than the SRs, or both. These VRs are found to be described by the templates, constructed as described above,

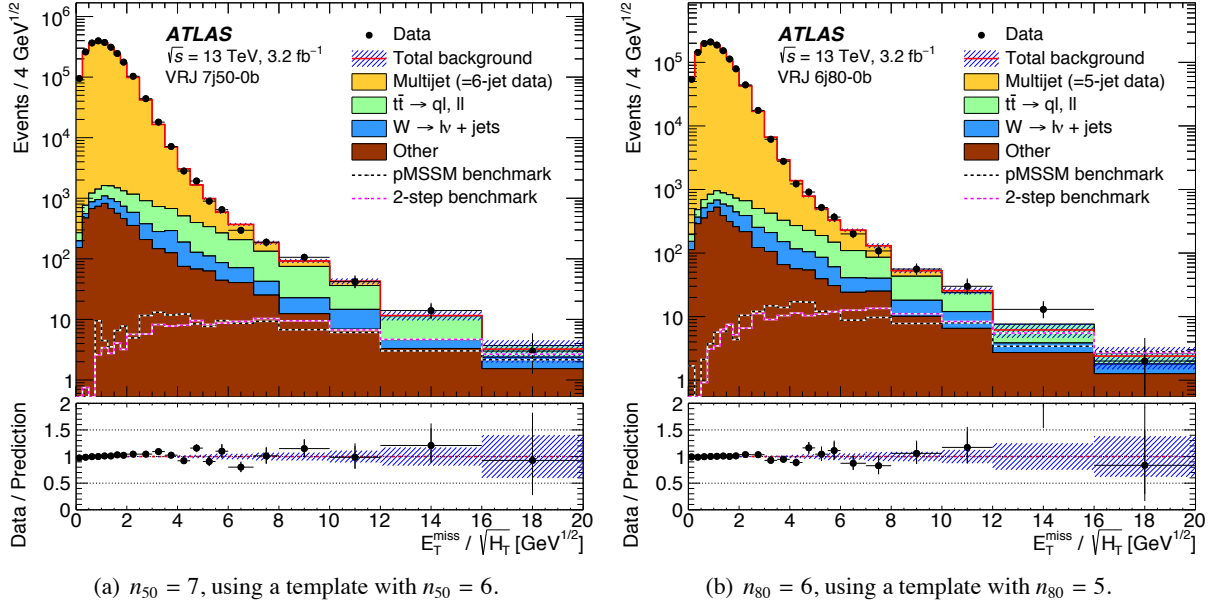


Figure 1: Example distributions of the ratio $E_T^{\text{miss}} / \sqrt{H_T}$ in the validation region with jet multiplicities (a) $n_{50} = 7$, and (b) $n_{80} = 6$. The templates, which are in each case built from a jet multiplicity one smaller than that of the data, are normalised to the data in the region with $E_T^{\text{miss}} / \sqrt{H_T} < 1.5 \text{ GeV}^{1/2}$. The templates are weighted by H_T as described in the text. No requirement is made on $n_{b\text{-jet}}$. Variable bin sizes are used with bin widths (in units of $\text{GeV}^{1/2}$) of 0.25 (up to $E_T^{\text{miss}} / \sqrt{H_T} = 2$), 0.5 (from 2 to 6), 1 (from 6 to 8), 2 (from 8 to 12) and 4 thereafter, with the last bin additionally containing all events with $E_T^{\text{miss}} / \sqrt{H_T} > 20 \text{ GeV}^{1/2}$. The total background can lie below the leptonic background contribution in individual bins, since the template can give a negative contribution. The dashed lines labelled ‘pMSSM’ and ‘2-step’ show the (small) signal contamination from the example SUSY models described in Section 4.2 – a pMSSM slice model with $(m_{\tilde{g}}, m_{\tilde{\chi}_1^0}) = (1300, 200) \text{ GeV}$ and a cascade decay model with $(m_{\tilde{g}}, m_{\tilde{\chi}_1^0}) = (1300, 200) \text{ GeV}$. The sub-plots show the ratio of the data to the SM prediction, with the blue hatched band showing the statistical uncertainty arising from a finite number of MC events and limited data in the templates and $E_T^{\text{miss}} / \sqrt{H_T} < 1.5$ normalisation regions.

mostly to within 10%–20%. However, for the tightest regions (with very few events) the discrepancy reaches 60%. The tests are performed separately for each of the three b -jet requirements, and the largest difference for each set, including VRs with jet multiplicity up to and including that of the SR in question, is included as an overall ‘closure’ systematic uncertainty associated with the method.

5 Statistical treatment and systematic uncertainties

Systematic uncertainties specific to the multijet and leptonic background contributions are described in Sections 4.3 and 4.1 respectively. Further uncertainties that apply to signal processes and all simulated backgrounds include those on the jet energy scale, jet resolution, integrated luminosity, the b -tagging efficiency (for correct and incorrect identifications of both the b - and non- b -jets), and the lepton identification efficiency and energy scale. They are in general small compared to the aforementioned ones, being at most one third the size of the largest of those.

SR name	<i>nj50</i> or <i>nj50-1b</i> or <i>nj50-2b</i>		<i>nj80</i> or <i>nj80-1b</i> or <i>nj80-2b</i>	
CR name	CR(<i>n</i> − 1) <i>j50-0b</i>	CR(<i>n</i> − 1) <i>j50-1b</i>	CR(<i>n</i> − 1) <i>j80-0b</i>	CR(<i>n</i> − 1) <i>j80-1b</i>
p_T^ℓ ($\ell \in \{e\mu\}$)	$> 20 \text{ GeV}$			
m_T	$< 120 \text{ GeV}$			
$E_T^{\text{miss}} / \sqrt{H_T}$	$> 3 \text{ GeV}^{1/2}$			
n_{50}^{CR}	$\geq n_{50} - 1$		—	
n_{80}^{CR}	—		$\geq n_{80} - 1$	
$n_{b\text{-jet}}$	0	≥ 1	0	≥ 1

Table 2: Leptonic control region definitions for each of the signal regions. In the names, the symbols n and $n - 1$ refer to the corresponding jet multiplicity requirements. For example the three signal regions $9j50$, $9j50-1b$ and $9j50-2b$ are each independently controlled by both the $\text{CR}9j50-0b$ and $\text{CR}9j50-1b$ control regions.

The effect of the systematic uncertainties on the SM background calculations is reduced by constraining the normalisations of the $t\bar{t}$ and W +jets backgrounds using dedicated control regions kinematically close to, but distinct from, the signal regions, as shown in Table 2. Each leptonic control region contains events with one electron or muon that meets the stricter requirements described in Section 2 and has transverse momentum $p_T^\ell > 20 \text{ GeV}$. There must be no additional lepton candidates with $p_T^\ell > 10 \text{ GeV}$. Each such region uses the same multijet trigger as its corresponding SR.

To reduce generic background from new particles which may decay to a final state with leptons and E_T^{miss} , a modest upper bound of 120 GeV is placed on the transverse mass $m_T = \left(2 E_T^{\text{miss}} p_T^\ell - 2 \vec{E}_T^{\text{miss}} \cdot \vec{p}_T^\ell\right)^{\frac{1}{2}}$. Since it is predominantly through hadronic τ decays that W bosons and $t\bar{t}$ pairs contribute to the signal regions, the corresponding control regions are created by recasting the muon or electron as a jet. If that lepton has sufficient p_T (without any additional calibration) it may contribute to the jet multiplicity count (denoted n_{50}^{CR} or n_{80}^{CR}), as well as to H_T and hence to $E_T^{\text{miss}} / \sqrt{H_T}$. In order to yield sufficient numbers of events in these CRs, the requirement on the jet multiplicity in each CR is one fewer than that in the corresponding SR, and a somewhat less stringent requirement is made on $E_T^{\text{miss}} / \sqrt{H_T}$ compared to the SRs.

For each SR (regardless of its own requirement on $n_{b\text{-jet}}$) there are two CRs, which require either exactly zero or at least one b -jet. These help constrain the combination of $t\bar{t}$ and W +jets backgrounds, with the $t\bar{t}$ background being enhanced in the CR that requires a b -jet. Figure 2 shows the resulting n_{50}^{CR} jet multiplicity distributions in these control regions.

For each signal region, a simultaneous fit is performed to the number of events found in the corresponding two CRs, using the HistFitter package [66]. For the purpose of exclusion, the simultaneous fit also includes data in the SR. In the fit the normalisations of the $t\bar{t}$ and W +jets background contributions are allowed to float, while the other leptonic backgrounds, which are generally subdominant, are determined directly from their yields using the corresponding theoretical cross-sections. The event yields in each CR and SR are assumed to be Poisson distributed. The systematic uncertainties are treated as Gaussian-distributed nuisance parameters, and are assumed to be correlated within each fit. The multijet background yield in the SR is determined separately from the data using the methods described in Section 4.3.

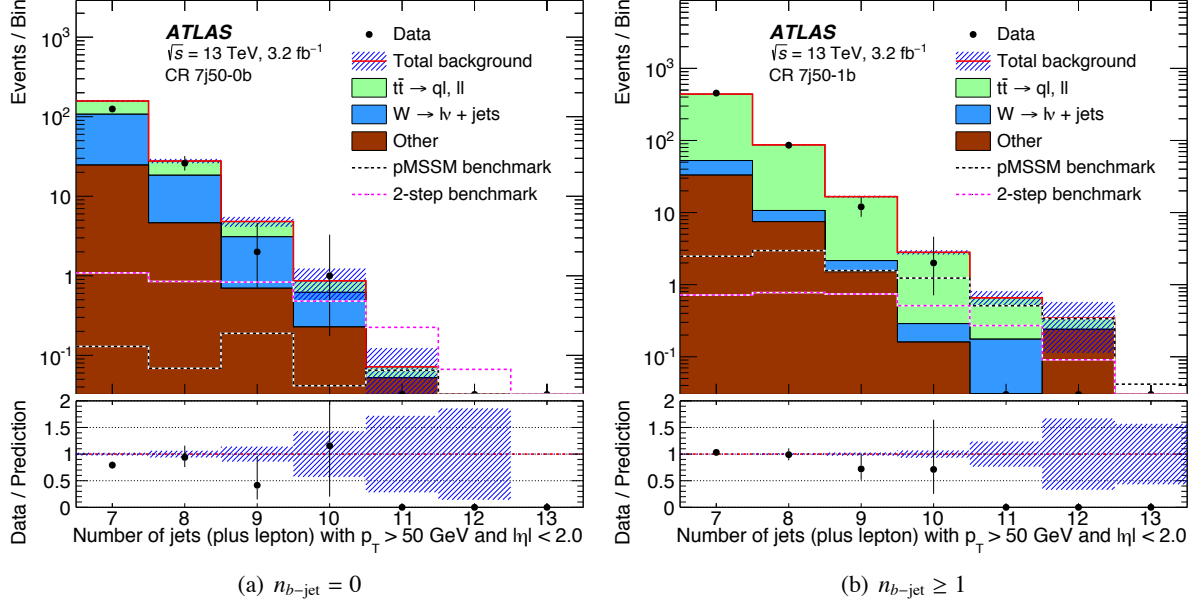


Figure 2: Control regions – requiring one lepton – showing the n_{50} jet multiplicity distributions after all selections aside from n_{50} . That lepton is permitted to contribute to the jet multiplicity count and to H_T . The sub-plots show the ratio of the data to the Standard Model prediction. The blue hatched bands on those sub-plots show MC statistical uncertainties. The dashed lines labelled ‘pMSSM’ and ‘2-step’ refer to benchmark signal points – a pMSSM slice model with $(m_{\tilde{g}}, m_{\tilde{\chi}_1^+}) = (1300, 200)$ GeV and a cascade decay model with $(m_{\tilde{g}}, m_{\tilde{\chi}_1^0}) = (1300, 200)$ GeV. All backgrounds are normalised according to their theoretical (pre-fit) cross-sections.

The normalisations for the $t\bar{t}$ and W +jets backgrounds are generally found to be consistent with their corresponding theoretical predictions when uncertainties are considered. Systematic uncertainties are larger than statistical uncertainties for the regions with looser selection criteria, with the situation reversed for those with tighter selection criteria. The systematic uncertainties with the largest impact include theoretical uncertainties on the $t\bar{t}$ background, the impact of limited numbers of events in the control regions, the closure of the multijet background estimation method and the jet energy scale. The overall post-fit values range from 14% to 42% with the theoretical uncertainties on the $t\bar{t}$ backgrounds typically being the most significant contribution.

6 Results

Figure 3 shows the post-fit $E_T^{\text{miss}}/\sqrt{H_T}$ distributions in the most sensitive signal regions (see below), while Figure 4 shows the background composition in all fifteen SRs. The background is split between multijet and leptonic processes, with the latter being 60–90% $t\bar{t}$.

The yields in each of the 15 signal regions are reported in Table 3. No significant excess is observed above the SM expectations in any SR, and most have confidence levels for the background-only hypothesis larger than 10%, as shown in Table 4. The table also shows the model-independent limits – 95% confidence level (CL) limits on the maximum contribution of new physics processes to the event yields in the various SRs, assuming zero signal contamination in control regions.

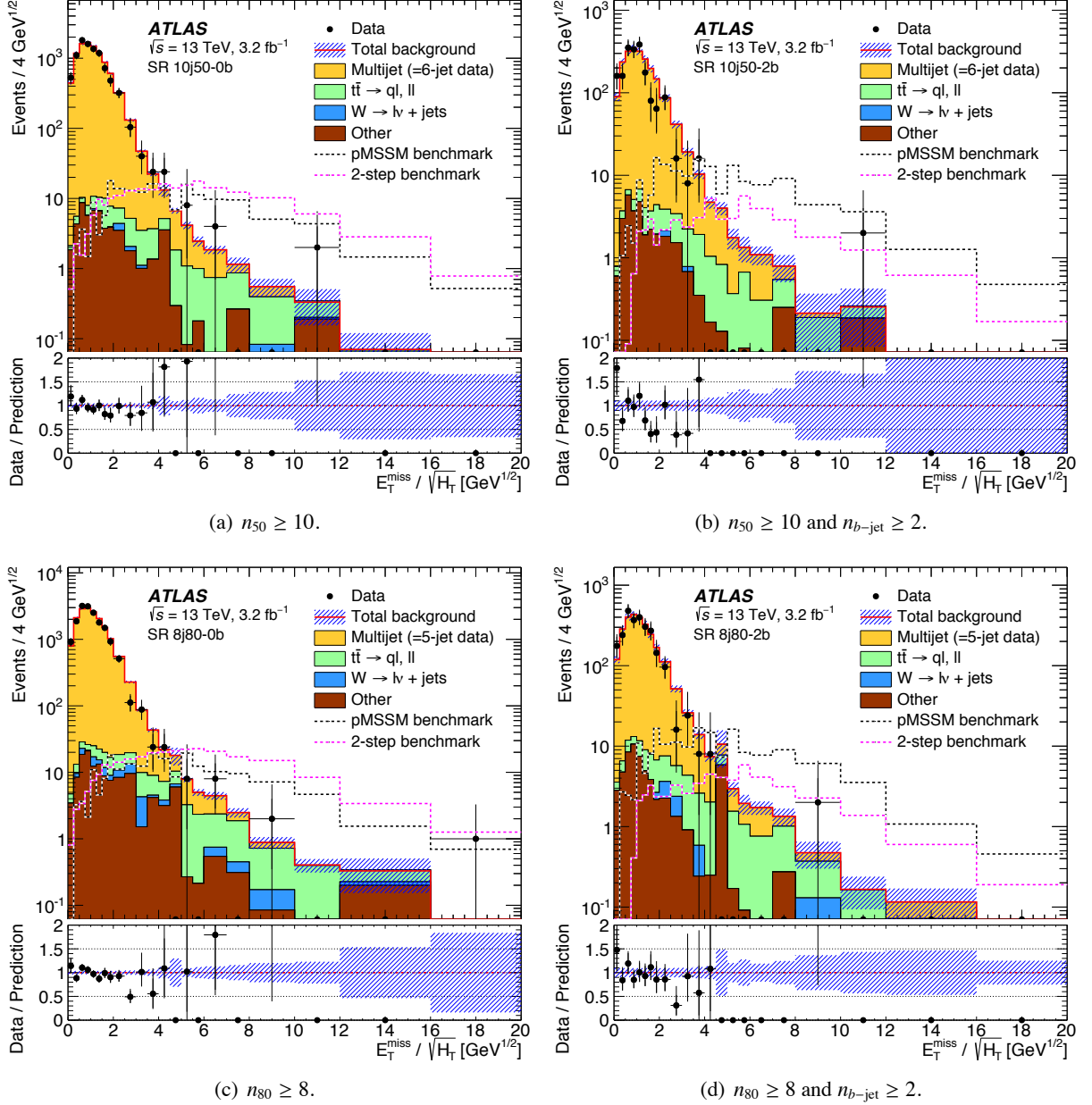
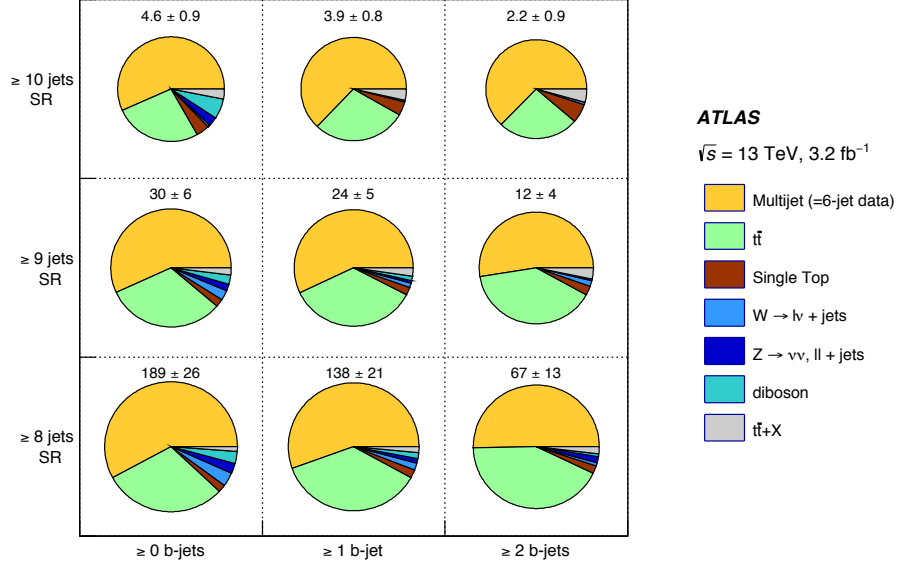
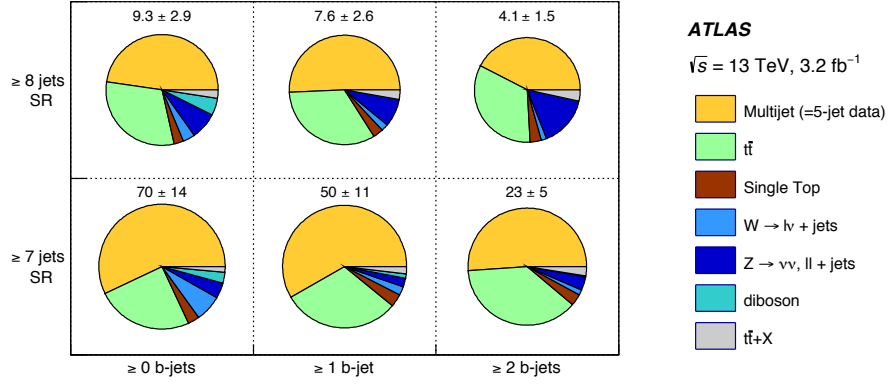


Figure 3: Example distributions of the selection variable $E_T^{\text{miss}} / \sqrt{H_T}$, for the largest multiplicities required of the number of jets with p_T larger than 50 GeV (top) or 80 GeV (bottom). The plots on the left have no selection on the number of b -tagged jets, while those on the right are for events with $n_{b\text{-jet}} \geq 2$. W +jets and $t\bar{t}$ are normalised to their post-fit values, while the other leptonic backgrounds are normalised to their theoretical cross-sections. The multijet templates are normalised to data at lower jet multiplicities in the region $E_T^{\text{miss}} / \sqrt{H_T} < 1.5 \text{ GeV}^{1/2}$, in the manner described in Section 4.3. The SRs lie where $E_T^{\text{miss}} / \sqrt{H_T} > 4 \text{ GeV}^{1/2}$. The dashed lines labelled ‘pMSSM’ and ‘2-step’ refer to benchmark signal points – a pMSSM slice model with $(m_{\tilde{g}}, m_{\tilde{\chi}_1^0}) = (1300, 200) \text{ GeV}$ and a cascade decay model with $(m_{\tilde{g}}, m_{\tilde{\chi}_1^0}) = (1300, 200) \text{ GeV}$. Other details are as described in Figure 1.



(a) n_{50}



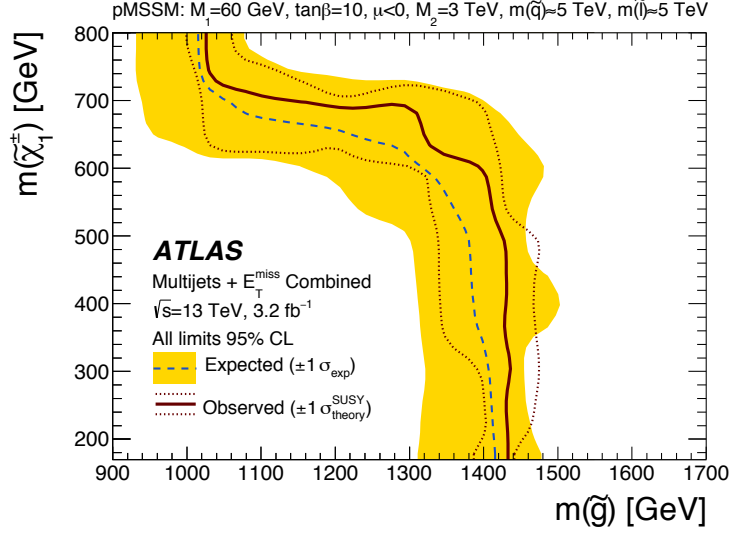
(b) n_{80}

Figure 4: Post-fit signal region compositions. The area of each pie chart is scaled to \log_{10} of the total expected yield (as printed above each one).

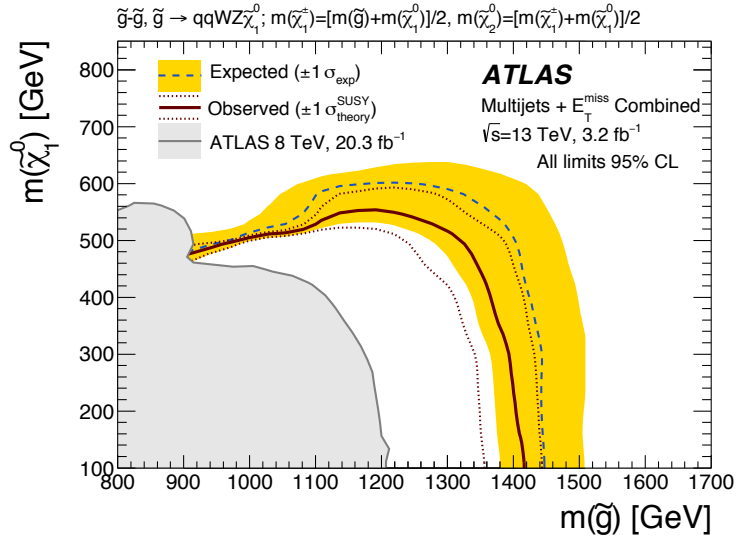
Signal region	Fitted background			Obs events
	Multijet	Leptonic	Total	
8j50	109.3 ± 6.9	80 ± 25	189 ± 26	157
8j50-1b	76.7 ± 2.7	62 ± 21	138 ± 21	97
8j50-2b	33.8 ± 2.1	33 ± 13	67 ± 13	39
9j50	16.8 ± 1.3	12.8 ± 5.4	29.6 ± 5.6	29
9j50-1b	13.5 ± 2.0	10.2 ± 4.9	23.8 ± 5.3	21
9j50-2b	6.4 ± 1.6	5.8 ± 3.3	12.1 ± 3.6	9
10j50	2.61 ± 0.61	1.99 ± 0.62	4.60 ± 0.87	6
10j50-1b	2.42 ± 0.62	1.44 ± 0.49	3.86 ± 0.79	3
10j50-2b	1.40 ± 0.87	0.83 ± 0.37	2.23 ± 0.94	1
7j80	40.0 ± 5.3	30 ± 13	70 ± 14	70
7j80-1b	29.1 ± 3.4	20.8 ± 10	50 ± 11	42
7j80-2b	11.5 ± 1.6	11.0 ± 5.0	22.5 ± 5.2	19
8j80	4.5 ± 1.9	4.9 ± 2.2	9.3 ± 2.9	8
8j80-1b	3.9 ± 1.5	3.8 ± 2.1	7.6 ± 2.6	4
8j80-2b	1.72 ± 0.93	2.3 ± 1.1	4.1 ± 1.5	2

Table 3: For each signal region, the expected SM background (and separately the multijet and leptonic contributions) and the observed number of data events. The SM background normalisations are obtained from fits to the data in control regions, as described in Sections 4 and 5. The signal regions are as defined in Table 1.

The results are interpreted in the context of the two supersymmetric models described in Section 4.2. The limit for each signal region is obtained by comparing the observed event count with that expected from Standard Model background plus SUSY signal processes, with their contamination of the leptonic control regions, typically below 10% for points close to the exclusion contour, being accounted for. All uncertainties on the Standard Model expectation are considered, including those which are correlated between signal and background (for instance jet energy scale uncertainties) and all, except theoretical cross-section uncertainties (PDF and scale), on the signal expectation. The resulting exclusion regions, shown in Figure 5, are obtained using the CL_s prescription [67]. For each signal model point, the signal region with the best expected limit is used. Signal regions defined by n_{50} and those defined by n_{80} both contribute to the best expected limit. The most sensitive signal regions are found to be those with no requirement on $n_{b\text{-jet}}$ for the simplified model decay. For the pMSSM slice, which has large branching ratios for gluinos to third-generation quarks, the best signal regions are those requiring either one or two b -jets. In both cases, gluino masses up to 1400 GeV are excluded at 95% confidence level, significantly extending previous limits for the simplified model decay.



(a) pMSSM slice



(b) Simplified cascade decay ('2-step') model

Figure 5: 95% CL exclusion curve for the two supersymmetric models described in the text. The solid red and dashed blue curves show the 95% CL observed and expected limits, respectively, including all uncertainties except the theoretical signal cross-section uncertainty (PDF and scale). The dotted red lines bracketing the observed limit represent the result produced when moving the signal cross-section by $\pm 1\sigma$ (as defined by the PDF and scale uncertainties). The shaded yellow band around the expected limit shows the $\pm 1\sigma$ variation of the expected limit. The shaded grey area shows the observed exclusion from the combination of ATLAS $\sqrt{s} = 8$ TeV analyses performed in Ref. [68] (Figure 25 therein). Excluded regions are below and to the left of the relevant lines.

Signal region	$\langle\epsilon\sigma\rangle_{\text{obs}}^{95}[\text{fb}]$	S_{obs}^{95}	S_{exp}^{95}	CL_B	$p(s=0)$
8j50	11	36	49^{+19}_{-13}	0.14	0.50
8j50-1b	6.8	22	37^{+13}_{-10}	0.04	0.50
8j50-2b	3.8	12	22^{+8}_{-6}	0.03	0.50
9j50	5.8	19	19^{+4}_{-5}	0.49	0.50
9j50-1b	5	16	17^{+2}_{-6}	0.38	0.50
9j50-2b	2.6	8	10^{+3}_{-2}	0.31	0.50
10j50	2.5	8	6^{+3}_{-1}	0.74	0.26
10j50-1b	1.6	5	6^{+2}_{-1}	0.37	0.50
10j50-2b	1.1	4	4^{+2}_{-1}	0.27	0.50
7j80	10	32	32^{+11}_{-9}	0.51	0.50
7j80-1b	6.2	20	24^{+6}_{-5}	0.29	0.50
7j80-2b	4.2	14	14^{+6}_{-2}	0.33	0.50
8j80	3.2	10	11^{+2}_{-4}	0.41	0.50
8j80-1b	1.7	5	7^{+3}_{-2}	0.20	0.50
8j80-2b	1.4	4	5^{+2}_{-1}	0.24	0.50

Table 4: The results of a fit to the control and signal region data, assuming no signal contamination in the control regions. Left to right: 95% CL upper limits on the visible cross-section ($\langle\epsilon\sigma\rangle_{\text{obs}}^{95}$) and on the number of signal events (S_{obs}^{95}). Convergence and stability tests of the fits suggest uncertainties of order 5% on S_{obs}^{95} resulting from these effects. The third column (S_{exp}^{95}) shows the 95% CL upper limit on the number of signal events, given the expected number (and $\pm 1\sigma$ excursions on the expectation) of background events. The last two columns indicate the CL_B value, i.e. the confidence level observed for the background-only hypothesis, and the discovery p -value ($p(s=0)$). The test is one-sided, so the p -value is 0.50 when the observed number of events is smaller than the prediction. Yields are not statistically independent, since there are correlated systematic uncertainties and since signal regions overlap.

7 Conclusions

A search is presented for new phenomena with large jet multiplicities (from ≥ 7 to ≥ 10) and missing transverse momentum. The search used 3.2 fb^{-1} of $\sqrt{s} = 13 \text{ TeV}$ pp collision data collected by the ATLAS experiment at the Large Hadron Collider. The increase in the LHC centre-of-mass energy provided increased sensitivity to higher-mass sparticles compared with previous searches. Further sensitivity was gained by considering separately final states with ≥ 0 , ≥ 1 and ≥ 2 b -tagged jets. The Standard Model predictions are found to be consistent with the data. The results are interpreted in the context of a simplified supersymmetry model, and a slice of the pMSSM, each of which predict cascade decays of supersymmetric particles and hence large jet multiplicities. The data exclude gluino masses up to 1400 GeV at the 95% CL in these models, significantly extending previous bounds. Model-independent limits were presented which allow reinterpretation of the results to cases of other models which also predict decays into multijet final states in association with invisible particles.

Acknowledgements

We thank CERN for the very successful operation of the LHC, as well as the support staff from our institutions without whom ATLAS could not be operated efficiently.

We acknowledge the support of ANPCyT, Argentina; YerPhI, Armenia; ARC, Australia; BMWFW and FWF, Austria; ANAS, Azerbaijan; SSTC, Belarus; CNPq and FAPESP, Brazil; NSERC, NRC and CFI, Canada; CERN; CONICYT, Chile; CAS, MOST and NSFC, China; COLCIENCIAS, Colombia; MSMT CR, MPO CR and VSC CR, Czech Republic; DNRF and DNSRC, Denmark; IN2P3-CNRS, CEA-DSM/IRFU, France; GNSF, Georgia; BMBF, HGF, and MPG, Germany; GSRT, Greece; RGC, Hong Kong SAR, China; ISF, I-CORE and Benoziyo Center, Israel; INFN, Italy; MEXT and JSPS, Japan; CNRST, Morocco; FOM and NWO, Netherlands; RCN, Norway; MNiSW and NCN, Poland; FCT, Portugal; MNE/IFA, Romania; MES of Russia and NRC KI, Russian Federation; JINR; MESTD, Serbia; MSSR, Slovakia; ARRS and MIZŠ, Slovenia; DST/NRF, South Africa; MINECO, Spain; SRC and Wallenberg Foundation, Sweden; SERI, SNSF and Cantons of Bern and Geneva, Switzerland; MOST, Taiwan; TAEK, Turkey; STFC, United Kingdom; DOE and NSF, United States of America. In addition, individual groups and members have received support from BCKDF, the Canada Council, CANARIE, CRC, Compute Canada, FQRNT, and the Ontario Innovation Trust, Canada; EPLANET, ERC, FP7, Horizon 2020 and Marie Skłodowska-Curie Actions, European Union; Investissements d’Avenir Labex and Idex, ANR, Région Auvergne and Fondation Partager le Savoir, France; DFG and AvH Foundation, Germany; Herakleitos, Thales and Aristeia programmes co-financed by EU-ESF and the Greek NSRF; BSF, GIF and Minerva, Israel; BRF, Norway; the Royal Society and Leverhulme Trust, United Kingdom.

The crucial computing support from all WLCG partners is acknowledged gratefully, in particular from CERN and the ATLAS Tier-1 facilities at TRIUMF (Canada), NDGF (Denmark, Norway, Sweden), CC-IN2P3 (France), KIT/GridKA (Germany), INFN-CNAF (Italy), NL-T1 (Netherlands), PIC (Spain), ASGC (Taiwan), RAL (UK) and BNL (USA) and in the Tier-2 facilities worldwide.

References

- [1] Y. A. Golfand and E. P. Likhtman, *Extension of the Algebra of Poincare Group Generators and Violation of p Invariance*, JETP Lett. **13** (1971) 323, [Pisma Zh.Eksp.Teor.Fiz.13:452-455,1971].
- [2] D. V. Volkov and V. P. Akulov, *Is the Neutrino a Goldstone Particle?*, Phys. Lett. **B 46** (1973) 109.
- [3] J. Wess and B. Zumino, *Supergauge Transformations in Four-Dimensions*, Nucl. Phys. **B 70** (1974) 39.
- [4] J. Wess and B. Zumino, *Supergauge Invariant Extension of Quantum Electrodynamics*, Nucl. Phys. **B 78** (1974) 1.
- [5] S. Ferrara and B. Zumino, *Supergauge Invariant Yang-Mills Theories*, Nucl. Phys. **B 79** (1974) 413.
- [6] A. Salam and J. A. Strathdee, *Supersymmetry and Nonabelian Gauges*, Phys. Lett. **B 51** (1974) 353.
- [7] G. R. Farrar and P. Fayet, *Phenomenology of the Production, Decay, and Detection of New Hadronic States Associated with Supersymmetry*, Phys. Lett. **B 76** (1978) 575.
- [8] ATLAS Collaboration, *Search for new phenomena in final states with large jet multiplicities and missing transverse momentum using $\sqrt{s} = 7$ TeV pp collisions with the ATLAS detector*, JHEP **11** (2011) 099, arXiv:1110.2299 [hep-ex].

- [9] ATLAS Collaboration, *Hunt for new phenomena using large jet multiplicities and missing transverse momentum with ATLAS in 4.7fb^{-1} of $\sqrt{s} = 7\text{ TeV}$ proton-proton collisions*, [JHEP **07** \(2012\) 167](#), arXiv:[1206.1760 \[hep-ex\]](#).
- [10] ATLAS Collaboration, *Search for new phenomena in final states with large jet multiplicities and missing transverse momentum at $\sqrt{s}=8\text{ TeV}$ proton-proton collisions using the ATLAS experiment*, [JHEP **10** \(2013\) 130](#), erratum [JHEP **01**\(2014\) 109](#), arXiv:[1308.1841 \[hep-ex\]](#).
- [11] ATLAS Collaboration, *The ATLAS Experiment at the CERN Large Hadron Collider*, [JINST **3** \(2008\) S08003](#).
- [12] ATLAS Collaboration, *Improved luminosity determination in pp collisions at $\sqrt{s} = 7\text{ TeV}$ using the ATLAS detector at the LHC*, [Eur. Phys. J. C **73** \(2013\) 2518](#), arXiv:[1302.4393 \[hep-ex\]](#).
- [13] M. Cacciari, G. P. Salam and G. Soyez, *The Anti- k_t jet clustering algorithm*, [JHEP **04** \(2008\) 063](#), arXiv:[0802.1189 \[hep-ph\]](#).
- [14] M. Cacciari and G. P. Salam, *Dispelling the N^3 myth for the k_t jet-finder*, [Phys. Lett. B **641** \(2006\) 57](#), arXiv:[hep-ph/0512210](#).
- [15] W. Lampl et al., *Calorimeter Clustering Algorithms: Description and Performance*, [ATL-LARG-PUB-2008-002](#) (2008), URL: <https://cds.cern.ch/record/1099735>.
- [16] ATLAS Collaboration, *Performance of pile-up mitigation techniques for jets in pp collisions at $\sqrt{s} = 8\text{ TeV}$ using the ATLAS detector* (2015), arXiv:[1510.03823 \[hep-ex\]](#).
- [17] ATLAS Collaboration, *Jet global sequential corrections with the ATLAS detector in proton-proton collisions at $\sqrt{s} = 8\text{ TeV}$* , [ATLAS-CONF-2015-002](#) (2015), URL: <https://cds.cern.ch/record/2001682>.
- [18] ATLAS Collaboration, *Jet Calibration and Systematic Uncertainties for Jets Reconstructed in the ATLAS Detector at $\sqrt{s} = 13\text{ TeV}$* , [ATL-PHYS-PUB-2015-015](#) (2015), URL: <https://cds.cern.ch/record/2037613>.
- [19] ATLAS Collaboration, *Selection of jets produced in 13 TeV proton-proton collisions with the ATLAS detector*, [ATLAS-CONF-2015-029](#) (2015), URL: <https://cds.cern.ch/record/2037702>.
- [20] ATLAS Collaboration, *Expected performance of the ATLAS b -tagging algorithms in Run-2*, [ATL-PHYS-PUB-2015-022](#) (2015), URL: <https://cds.cern.ch/record/2037697>.
- [21] ATLAS Collaboration, *Commissioning of the ATLAS b -tagging algorithms using $t\bar{t}$ events in early Run-2 data*, [ATL-PHYS-PUB-2015-039](#) (2015), URL: <https://cds.cern.ch/record/2047871>.
- [22] ATLAS Collaboration, *Electron identification measurements in ATLAS using $\sqrt{s} = 13\text{ TeV}$ data with 50 ns bunch spacing*, [ATL-PHYS-PUB-2015-041](#) (2015), URL: <https://cds.cern.ch/record/2048202>.
- [23] ATLAS Collaboration, *Muon reconstruction performance in early $\sqrt{s} = 13\text{ TeV}$ data*, [ATL-PHYS-PUB-2015-037](#) (2015), URL: <https://cds.cern.ch/record/2047831>.
- [24] ATLAS Collaboration, *Expected performance of missing transverse momentum reconstruction for the ATLAS detector at $\sqrt{s} = 13\text{ TeV}$* , [ATL-PHYS-PUB-2015-023](#) (2015), URL: <https://cds.cern.ch/record/2037700>.

- [25] T. Sjöstrand, S. Mrenna and P. Z. Skands, *A Brief Introduction to PYTHIA 8.1*, *Comput. Phys. Commun.* **178** (2008) 852, arXiv:0710.3820 [hep-ph].
- [26] ATLAS Collaboration, *Summary of ATLAS Pythia 8 tunes*, ATL-PHYS-PUB-2012-003 (2012), URL: <https://cds.cern.ch/record/1474107>.
- [27] A. D. Martin, W. J. Stirling, R. S. Thorne and G. Watt, *Parton distributions for the LHC*, *Eur. Phys. J. C* **63** (2009) 189–285, arXiv:0901.0002 [hep-ph].
- [28] ATLAS Collaboration, *The ATLAS Simulation Infrastructure*, *Eur. Phys. J. C* **70** (2010) 823, arXiv:1005.4568 [physics.ins-det].
- [29] GEANT4 Collaboration, S. Agostinelli et al., *GEANT4: A simulation toolkit*, *Nucl. Instrum. Meth. A* **506** (2003) 250.
- [30] ATLAS Collaboration, *Performance of the Fast ATLAS Tracking Simulation (FATRAS) and the ATLAS Fast Calorimeter Simulation (FastCaloSim) with single particles*, ATL-SOFT-PUB-2014-001 (2014), URL: <http://cds.cern.ch/record/1669341>.
- [31] ATLAS Collaboration, *Simulation of top quark production for the ATLAS experiment at $\sqrt{s} = 13$ TeV*, ATL-PHYS-PUB-2016-004 (2016), URL: <https://cds.cern.ch/record/2120417>.
- [32] S. Alioli et al., *A general framework for implementing NLO calculations in shower Monte Carlo programs: the POWHEG BOX*, *JHEP* **06** (2010) 043, arXiv:1002.2581 [hep-ph].
- [33] H.-L. Lai et al., *New parton distributions for collider physics*, *Phys. Rev. D* **82** (2010) 074024, arXiv:1007.2241 [hep-ph].
- [34] P. Artoisenet et al., *Automatic spin-entangled decays of heavy resonances in Monte Carlo simulations*, *JHEP* **03** (2013) 015, arXiv:1212.3460 [hep-ph].
- [35] T. Sjöstrand, S. Mrenna and P. Z. Skands, *PYTHIA 6.4 physics and manual*, *JHEP* **05** (2006) 026, arXiv:hep-ph/0603175.
- [36] J. Pumplin et al., *New generation of parton distributions with uncertainties from global QCD analysis*, *JHEP* **07** (2002) 012, arXiv:hep-ph/0201195.
- [37] P. Z. Skands, *Tuning Monte Carlo Generators: The Perugia Tunes*, *Phys. Rev. D* **82** (2010) 074018, arXiv:1005.3457 [hep-ph].
- [38] D. J. Lange, *The EvtGen particle decay simulation package*, *Nucl. Instrum. Meth. A* **462** (2001) 152.
- [39] M. Czakon and A. Mitov, *Top++: a program for the calculation of the top-pair cross-section at hadron colliders*, *Comput. Phys. Commun.* **185** (2014) 2930, arXiv:1112.5675 [hep-ph].
- [40] ATLAS Collaboration, *Modelling of the $t\bar{t}H$ and $t\bar{t}V$ ($V = W, Z$) processes for $\sqrt{s} = 13$ TeV ATLAS analyses*, ATL-PHYS-PUB-2016-005 (2016), URL: <https://cds.cern.ch/record/2120826>.
- [41] J. Alwall et al., *The automated computation of tree-level and next-to-leading order differential cross sections, and their matching to parton shower simulations*, *JHEP* **07** (2014) 079, arXiv:1405.0301 [hep-ph].

- [42] ATLAS Collaboration, *ATLAS Run 1 Pythia8 tunes*, ATL-PHYS-PUB-2014-021 (2014), URL: <https://cds.cern.ch/record/1966419>.
- [43] NNPDF Collaboration, R. D. Ball et al., *Parton distributions with LHC data*, Nucl. Phys. B **867** (2013) 244, arXiv:1207.1303 [hep-ph].
- [44] ATLAS Collaboration, *Monte Carlo Generators for the Production of a W or Z/ γ^* Boson in Association with Jets at ATLAS in Run 2*, ATL-PHYS-PUB-2016-003 (2016), URL: <https://cds.cern.ch/record/2120133>.
- [45] R. Gavin, Y. Li, F. Petriello and S. Quackenbush, *FEWZ 2.0: A code for hadronic Z production at next-to-next-to-leading order*, Comput. Phys. Commun. **182** (2011) 2388, arXiv:1011.3540 [hep-ph].
- [46] ATLAS Collaboration, *Multi-Boson Simulation for 13 TeV ATLAS Analyses*, ATL-PHYS-PUB-2016-002 (2016), URL: <https://cds.cern.ch/record/2119986>.
- [47] T. Gleisberg et al., *Event generation with SHERPA 1.1*, JHEP **02** (2009) 007, arXiv:0811.4622 [hep-ph].
- [48] T. Gleisberg and S. Hoeche, *Comix, a new matrix element generator*, JHEP **12** (2008) 039, arXiv:0808.3674 [hep-ph].
- [49] F. Cascioli, P. Maierhöfer and S. Pozzorini, *Scattering Amplitudes with Open Loops*, Phys. Rev. Lett. **108** (2012) 111601, arXiv:1111.5206 [hep-ph].
- [50] S. Schumann and F. Krauss, *A Parton shower algorithm based on Catani-Seymour dipole factorisation*, JHEP **03** (2008) 038, arXiv:0709.1027 [hep-ph].
- [51] S. Hoeche et al., *QCD matrix elements + parton showers: The NLO case*, JHEP **04** (2013) 027, arXiv:1207.5030 [hep-ph].
- [52] ATLAS Collaboration, *Comparison of Monte Carlo generator predictions from Powheg and Sherpa to ATLAS measurements of top pair production at 7 TeV*, ATL-PHYS-PUB-2015-011 (2015), URL: <https://cds.cern.ch/record/2020602>.
- [53] M. Bähr et al., *Herwig++ Physics and Manual*, Eur. Phys. J. C **58** (2008) 639, arXiv:0803.0883 [hep-ph].
- [54] A. Djouadi et al., *The Minimal supersymmetric standard model: Group summary report* (1998), arXiv:hep-ph/9901246.
- [55] C. F. Berger, J. S. Gainer, J. L. Hewett and T. G. Rizzo, *Supersymmetry Without Prejudice*, JHEP **02** (2009) 023, arXiv:0812.0980 [hep-ph].
- [56] ATLAS Collaboration, *Summary of the ATLAS experiment's sensitivity to supersymmetry after LHC Run 1 — interpreted in the phenomenological MSSM*, JHEP **10** (2015) 134, arXiv:1508.06608 [hep-ex].
- [57] B. C. Allanach, *SOFTSUSY: a program for calculating supersymmetric spectra*, Comput. Phys. Commun. **143** (2002) 305, arXiv:hep-ph/0104145.
- [58] A. Djouadi, M. Mühlleitner and M. Spira, *Decays of supersymmetric particles: The Program SUSY-HIT (SUSpect-SdecaY-Hdecay-InTerface)*, Acta Phys. Polon. B **38** (2007) 635, arXiv:hep-ph/0609292.
- [59] Soon to appear on HepData: <http://hepdata.cedar.ac.uk>.

- [60] W. Beenakker, R. Höpkerb, M. Spirac and P. M. Zerwas,
Squark and gluino production at hadron colliders, *Nucl.Phys. B* **492** (1997) 51,
arXiv:[hep-ph/9610490](#) [[hep-ph](#)].
- [61] A. Kulesza and L. Motyka,
Threshold resummation for squark-antisquark and gluino-pair production at the LHC,
Phys.Rev.Lett. **102** (2009) 111802, arXiv:[0807.2405](#) [[hep-ph](#)].
- [62] A. Kulesza and L. Motyka, *Soft gluon resummation for the production of gluino-gluino and squark-antisquark pairs at the LHC*, *Phys.Rev. D* **80** (2009) 095004,
arXiv:[0905.4749](#) [[hep-ph](#)].
- [63] W. Beenakker et al., *Soft-gluon resummation for squark and gluino hadroproduction*,
JHEP **12** (2009) 041, arXiv:[0909.4418](#) [[hep-ph](#)].
- [64] W. Beenakker et al., *Squark and gluino hadroproduction*, *Int. J. Mod. Phys. A* **26** (2011) 2637,
arXiv:[1105.1110](#) [[hep-ph](#)].
- [65] M. Krämer et al., *Supersymmetry production cross sections in pp collisions at $\sqrt{s} = 7$ TeV* (2012),
arXiv:[1206.2892](#) [[hep-ph](#)].
- [66] M. Baak et al., *HistFitter software framework for statistical data analysis*,
Eur. Phys. J. C **75** (2015) 153, arXiv:[1410.1280](#) [[hep-ex](#)].
- [67] A. Read, *Presentation of search results: the CL_s technique*, *J. Phys. G* **28** (2002) 2693–2704.
- [68] ATLAS Collaboration, *Summary of the searches for squarks and gluinos using $\sqrt{s} = 8$ TeV pp collisions with the ATLAS experiment at the LHC*, *JHEP* **10** (2015) 054,
arXiv:[1507.05525](#) [[hep-ex](#)].

Cutflow for two supersymmetric models; a 'two-step' model where the gluinos have a mass of 1300 GeV and the lightest neutralinos have a mass of 200 GeV (20,000 events generated); and a 'pMSSM' model, where the gluinos have a mass of 1300 GeV and the lightest chargino have a mass of 200 GeV (25,000 events generated). 'Preselection' roughly equates to selecting events with a total (jet plus lepton) multiplicity of six or higher, and 'Additional ETmiss Cleaning' refers to the $\Delta\phi(\text{jet}, E_{\text{T}}^{\text{miss}})$ and dead calorimeter module cuts described in Section 2. The numbers are normalised to a luminosity of 3.21 fb⁻¹. The b-jet requirements are made separately, as in the signal region definitions.

	Two-step $[\tilde{g}, \tilde{\chi}_1^0] : [1300, 200] \text{ [GeV]}$	pMSSM $[\tilde{g}, \tilde{\chi}_1^\pm] : [1300, 200] \text{ [GeV]}$
Number of Events ($L_{\text{int}} = 3.21 \text{ fb}^{-1}$)	147.8	147.8
Preselection	147.0	147.6
Event Cleaning	144.7	146.3
Additional $E_{\text{T}}^{\text{miss}}$ Cleaning	139.9	141.6
Lepton Veto	77.9	70.7
6j50 $ \eta < 2.0$	73.5	62.6
Trigger (6 jets with $E_{\text{T}} > 45 \text{ GeV}$, $ \eta < 2.4$)	73.4	62.6
8j50, $ \eta < 2.0$	50.9	37.0
$E_{\text{T}}^{\text{miss}}/\sqrt{H_{\text{T}}} > 4.0 \text{ GeV}^{1/2}$	39.7	26.4
& ≥ 0 bjet	39.7	26.4
& ≥ 1 bjet	19.2	25.5
& ≥ 2 bjet	6.9	21.0
9j50, $ \eta < 2.0$	33.5	24.4
$E_{\text{T}}^{\text{miss}}/\sqrt{H_{\text{T}}} > 4.0 \text{ GeV}^{1/2}$	25.8	16.7
& ≥ 0 bjet	25.8	16.7
& ≥ 1 bjet	12.9	16.3
& ≥ 2 bjet	4.8	13.8
10j50, $ \eta < 2.0$	17.6	13.5
$E_{\text{T}}^{\text{miss}}/\sqrt{H_{\text{T}}} > 4.0 \text{ GeV}^{1/2}$	13.1	8.8
& ≥ 0 bjet	13.1	8.8
& ≥ 1 bjet	6.9	8.6
& ≥ 2 bjet	3.1	7.5
5j80 $ \eta < 2.0$	72.4	59.9
Trigger (5 jets with $E_{\text{T}} > 70 \text{ GeV}$)	72.3	59.8
7j80, $ \eta < 2.0$	43.1	29.1
$E_{\text{T}}^{\text{miss}}/\sqrt{H_{\text{T}}} > 4.0 \text{ GeV}^{1/2}$	33.4	20.3
& ≥ 0 bjet	33.4	20.3
& ≥ 1 bjet	16.3	19.5
& ≥ 2 bjet	5.9	15.9
8j80, $ \eta < 2.0$	24.2	15.2
$E_{\text{T}}^{\text{miss}}/\sqrt{H_{\text{T}}} > 4.0 \text{ GeV}^{1/2}$	18.3	10.1
& ≥ 0 bjet	18.3	10.1
& ≥ 1 bjet	9.1	9.9
& ≥ 2 bjet	3.3	8.2